Journal of Earth Sciences and Geotechnical Engineering, Vol. 9, No. 3, 2019, 133-163
ISSN: 1792-9040 (print version), 1792-9660 (online)
Scientific Press International Limited

Bentonite Homogenisation – Modelling of Homogenisation Processes in Bentonite Buffer Materials in Repositories

Lennart Börgesson[1], Ann Dueck[2] and Jan Hernelind[3]

Abstract

Swelling and homogenisation of bentonite materials are important functions of the bentonite to guarantee the requirements of the buffer and backfill after full water saturation in deposition holes and tunnels in a radioactive waste repository. A study including a laboratory testing programme with tests in different scales and complexity and modelling of the tests is financed by SKB.
In this article modelling of some of the laboratory tests with analytical methods and with finite element calculations is described and evaluated. The laboratory tests and the results are described in another article by Dueck et al [1].
The FE-program Abaqus has been used to model four of the homogenisation tests with two different mechanical material models. Two different plastic material models (Drucker-Prager and Claytech Plastic Cap) have been used.
Two fundamental tests with only axial or radial swelling were modelled to check the models and calibrate the parameters of the models. Both these tests were very well modelled with the Cap model but less good with the Drucker-Prager model.
Ten almost identical tests of the homogenisation of two bentonites with large density differences placed in long tubes with raw surfaces are running with the purpose to study long term homogenisation. One of those have been terminated and sampled and was modelled with an analytical solution. The results showed that the homogenisation was well captured if the residual friction angle evaluated from friction tests was used. Finally, homogenisation of a large bentonite block with two cavities was modelled with Abaqus. The calculation worked well but the model underestimated the self-healing ability.

[1] Clay Technology AB, Sweden
[2] Clay Technology AB, Sweden
[3] Scanscot AB, Sweden

Article Info: *Received:* June 5, 2019. *Revised:* August 23, 2019.
Published online: September 10, 2019.

Keywords: Bentonite, homogenisation, modelling, swelling tests, void ratio, dry density, angle of friction.

1. Introduction

1.1 Background

Swelling and homogenisation of bentonite materials are important functions of the bentonite to guarantee the requirements of the buffer and backfill after full water saturation in deposition holes and tunnels in a repository. It is important to understand and be able to predict the final condition of the buffer after the swelling and homogenisation, which occurs both during the initial saturation and homogenisation of the buffer, which according to the KBS-3 concept consists of blocks and pellets, and also after possible loss of bentonite caused by for example erosion.

To increase the knowledge of the homogenisation process SKB has initiated and financed a homogenisation project that has been running during several years. The project consists of several parts; theoretical studies and modelling, fundamental laboratory swelling tests, laboratory study of the influence of friction, medium scale tests of a scenario involving loss of bentonite and long tubes tests with large density gradients.

Material models have been developed and verified with some of the laboratory test results from this project. Modelling of the swelling bentonite based on and compared to test results from the buffer homogenisation project has been presented by Börgesson et al [2] and Dueck et al [3].

A new hydro-mechanical material model, intended for bentonite-based components, has also been developed and implemented into the COMSOL Multiphysics platform (Dueck et al [3]) but is not described in this article.

1.2 The homogenisation project

How well the bentonite self-seals and homogenises is investigated in the homogenisation project. The laboratory tests have mainly been made on specimens that have been water saturated or close to water saturated from start, which means that the saturation process has not been included in the tests.

The purposes of the project and the tests have been to

- understand how homogenisation evolves and ends,
- investigate the different factors influencing homogenisation,
- understand how much remaining inhomogeneities that may prevail in bentonite,
- be a base for creating hydro-mechanical models for the homogenisation process,
- evaluate model parameters,
- confirm the models and calculation tools by modelling different homogenisation cases.

The laboratory tests made in this project have been divided into four parts

- fundamental swelling tests to increase the knowledge about material parameters
- measurement of friction between bentonite and other surfaces
- homogenisation in long tubes where the effect of time also can be studied
- homogenisation after loss of bentonite in the self-healing tests

The modelling related to the laboratory test results from this project has included comparison with measured results and has mainly been concentrated on

- evaluation of models and model parameters and verification of the models by modelling the fundamental swelling tests,
- analyses and modelling of one test from the series with long tubes
- modelling of one of the self-healing tests
- development of a new hydro-mechanical model for COMSOL

1.3 Modelling described in this article

The modelling of the following four laboratory tests will be described in this article:
Test HR-A1, which is a fundamental test with axial swelling
Test HR-Ro1, which is a fundamental test with radial outwards swelling
Test FLR5, which is a test in long tubes with large density differences
Test SH1, which is a test with two large cavities in a complicated geometry
The tests will be briefly described in this article but are in more detail described by Dueck et al [4, 5, 6, 7, 3, 1].

2. Finite element code and material models

2.1 General

Three tests are modelled with the finite element code Abaqus. The code and the material model used for SR-Site are described by Åkesson et al [8, 9]. The material models used for the present tests are described in detail by Börgesson et al [10]. The code is also described by Börgesson et al [11, 12].
The material models are coupled hydro-mechanical with the effective stress theory as base. Full water saturation is assumed for these models. The hydraulic model use Darcy's law with hydraulic conductivity modelled as a function of the void ratio.
Two mechanical material models have been used. Both models are elastic-plastic models and use porous elasticity for the elastic model. One of the plastic models uses Drucker-Prager plasticity while the other one is a Plastic Cap model derived and described by Börgesson et al [10].
The parameters of the original Claytech Plastic Cap model were slightly modified when modelling test HR-A1. The final model is described here.

2.2 Hydraulic model

The hydraulic conductivity k is modelled as a function of the void ratio e according to Table 1.

Table 1: Hydraulic conductivity as a function of void ratio

e	K [m/s]
0.45	0.5×10^{-14}
0.70	$4.0 \cdot 10^{-14}$
1.00	$2.0 \cdot 10^{-13}$
1.5	$1.0 \cdot 10^{-12}$
2.00	$0.5 \cdot 10^{-11}$
3.00	$1.0 \cdot 10^{-11}$
5.00	$3.5 \cdot 10^{-11}$
10.00	$1.5 \cdot 10^{-10}$
20.00	$0.75 \cdot 10^{-9}$

2.3 Mechanical models

Porous Elastic implies a logarithmic relation between the void ratio e and the average effective stress p according to Equation 1.

$$\Delta e = -\kappa \cdot \Delta \ln p \tag{1}$$

where κ = porous bulk modulus
Poisson's ratio ν is also required.
The following values have been used:
$\kappa = 0.175$
$\nu = 0.3$

Equation 1 is not valid for very low densities (see Börgesson et al [10]) but only in the interval $0.7<e<1.5$, which correspond to 1110 kg/m^3<ρ_d<1635 kg/m^3. At lower densities the porous bulk modulus is much larger ($\kappa \approx 1.37$) but this change in modulus is not included in the model. If swelling causes a lower density the swelling has to be corrected for that part.

Drucker-Prager Plasticity contains the following parameters:

β = friction angle in the p-q plane
d = cohesion in the p-q plane
Ψ = dilation angle
$q = f(\varepsilon^d_{pl})$ = yield function

The parameter values in this model are as follows:

$\beta = 17°$
$d = 100$ kPa
$\Psi = 2°$
$q = f(\varepsilon_{pl})$

Yield function: see Table 2.

Table 2: Yield function

q (kPa)	ε_{pl}
112	0
138	0.005
163	0.02
188	0.04
213	0.1

Figure 1 illustrates the Drucker-Prager model.

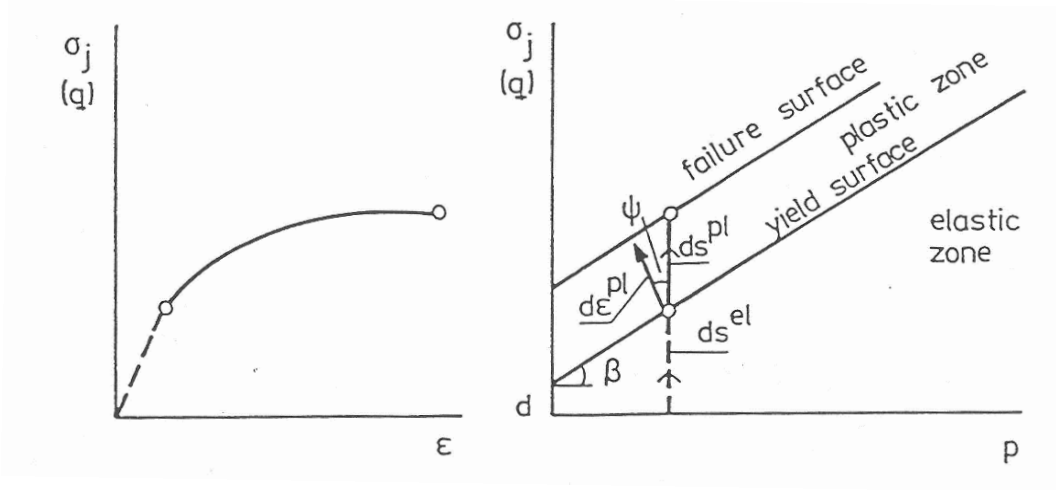

Figure 1: Illustration of the Drucker-Prager model.

The Claytech Plastic Cap model and its background are described in detail by Börgesson et al [10]. An overview of the model and its parameters are given in Figure 2.

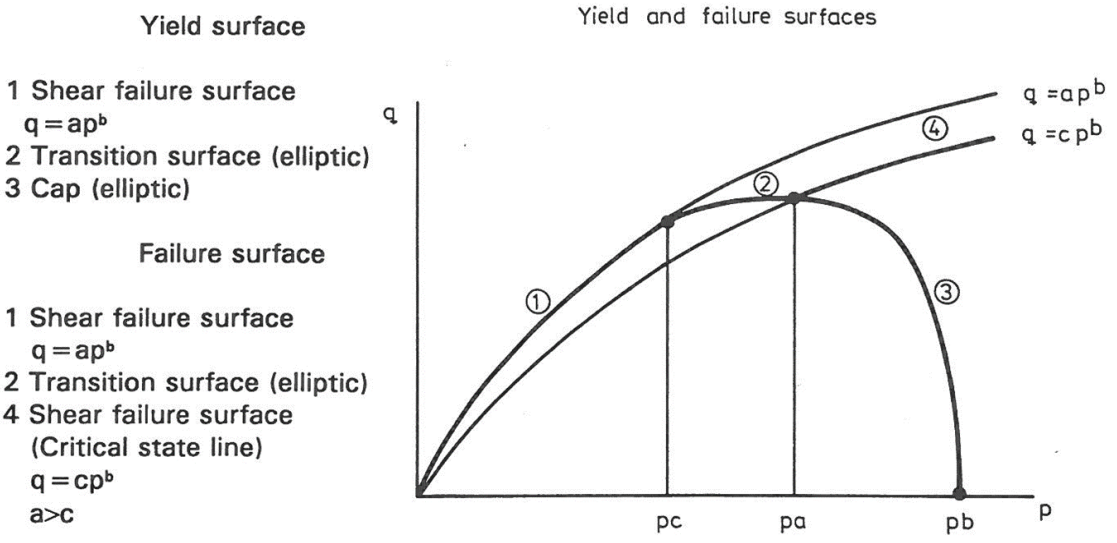

Figure 2: Overview of the Claytech Plastic Cap model.

The parameters of the model slightly revised from the initial values are
a = 2.45
c = 2.20
b = 0.77
K= 1.0 (influence of the intermediate principal stress on q at failure)
γ = 0.1 (ratio of the two axes in the elliptic transition surface (yield surface 2))
R = 0.1 (ratio of the two axes in the elliptic cap (yield surface 3)
p_b = 30000 kPa
p_f = -25000 kPa (intersection between the elliptic flow surface and the p-axis at p<0)
Cap hardening = see Table 3

Table 3: Cap hardening function

p kPa	$^{e}\log(1+\varepsilon^{v}_{pl})$
100	0
331	0.1133
934	0.2112
2160	0.2904
3247	0.3289
4294	0.3553
8240	0.4169
10044	0.4356
12530	0.4565
13299	0.4621
17562	0.4884
30000	0.5390

2.4 Contact properties

The shear resistance between bentonite and an outer surface has been investigated with a large number of friction tests described by Dueck et al [3], which show that the friction angle is about half the friction angle of the bentonite itself. As an average (depending on the swelling pressure and surface type) the friction angle 5-7º has been used in the modellings.

3. Fundamental swelling tests from the HR-series

3.1 General

Four different fundamental test types have been modelled, namely axial swelling, radial outwards swelling, radial inwards swelling and isotropic swelling. The axial swelling test was used for checking and calibrating the material models and the other tests were used to evaluate the derived model. Two of them will be described here.

3.2 Axial swelling

The axial swelling test HR-A1 was at first used to check and calibrate the models. The test is in more detail described by Dueck et al [3, 1]. The Drucker-Prager model could not yield an acceptable result regarding the swelling pressure evolution and the final gradient in density that occurred after equilibrated swelling. Instead the Claytech Plastic Cap model was used with parameter values derived at that time. However, in order to get the best agreement between measured and modelled results the parameters of the elastic model, the plastic model and the hydraulic conductivity had to be somewhat changed to the values shown above.

In this test the axial swelling pressure was measured on the upper piston and the radial pressure was measured in three points (Dueck et al [3]). After termination of the test the specimen was sliced and the density distribution in axial direction determined.

The finite element mesh is shown in Figure 3.

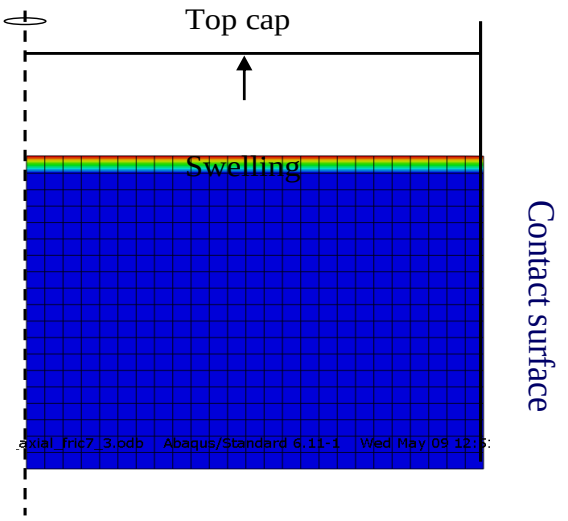

Figure 3: Element mesh for the axial swelling test. Axial symmetry at the left side and contact surfaces at the other sides.

Geometry:

- Radius: 50 mm
- Start height: 37.4 mm
- End height: 50 mm

Start properties: u_0=-10MPa, e_0=0.70; ρ_{d0}=1635 kg/m^3
End average properties: u=0MPa, e=1.22; ρ_d=1250 kg/m^3
Swelling $\Delta V/V$=33.6%
Swelling with water available at the top surface
Radial contact surface with friction ϕ=7°

Figures 4 and 5 show comparison between modelled results and measured results. The results agree rather well. The difference between the modelled densities in the centre and at the outer boundary is caused by the friction against the oedometer ring. The modelled final average dry density is a little lower than the measured, which obviously must be caused by too low initial dry density in the model. So, the modelled stresses are logically lower than the measured.

Some observations:

The initial phase of the stress evolution (10-20 days) agrees very well for the radial stress at 30 mm with a peak stress very early and then a decrease in stress followed by a new increase in stress. This phenomenon is also modelled for the stress at 15 mm.

The radial stress evolution at 45 mm and the axial stress distribution on top of the oedometer differ significantly from the measured during the first 20 days. According to the measurements the stress starts increasing very early while the modelled stress is very low and the axial stress zero during the first 20 days. The reason for this difference is probably mainly caused by the porous elastic modulus κ at high void ratios as pointed out earlier. The early swelling is strongly underestimated.

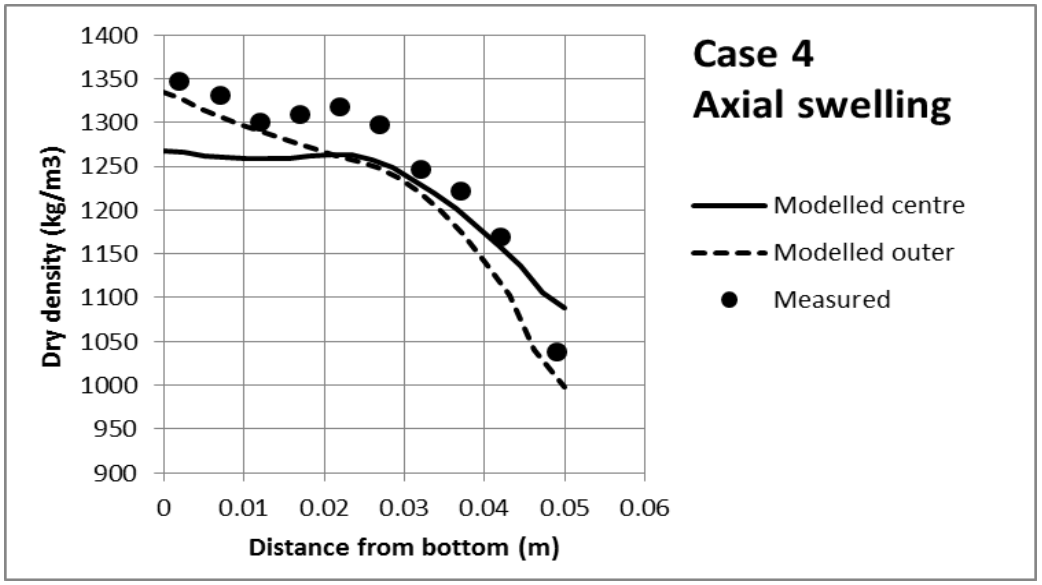

Figure 4: Results from the Plastic Cap model. Modelled density distribution along the center axis and along the periphery (outer) and measured average density distribution.

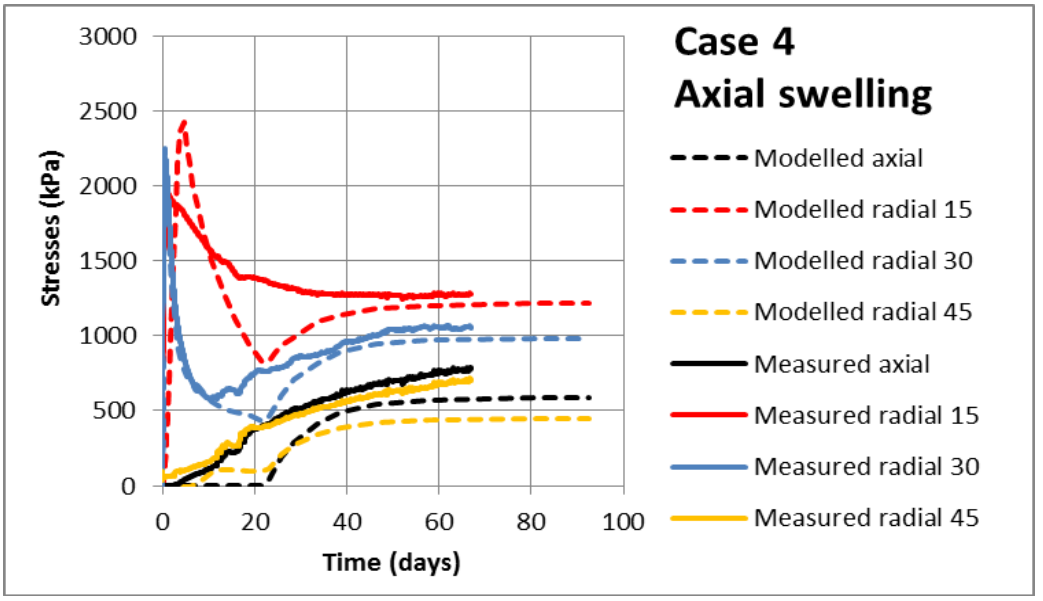

Figure 5: Results from the Plastic Cap model. Modelled and measured evolution of normal stress.

3.3 Radial outwards swelling

The calibrated model was checked by modelling the radial outwards swelling test HR-Ro1 described by Dueck et al [3, 1].

The mesh is shown in Figure 6.

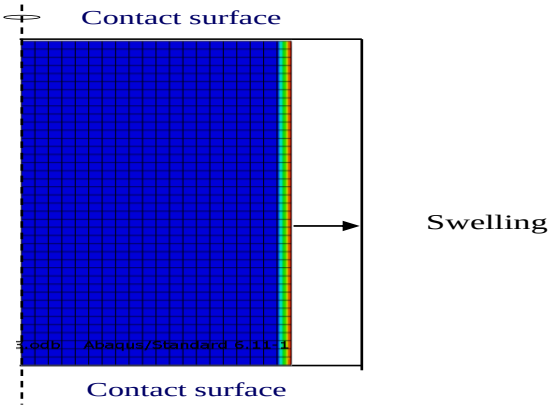

Figure 6: Element mesh for the radial swelling test. Axial symmetry at the left side and contact surfaces at the other side.

Geometry:

- Height: 80 mm
- Start radius: 40.5 mm
- End radius: 48.5 mm

Start properties: u_0=-10MPa, e_0=0.70; ρ_{d0}=1635 kg/m^3
End average properties: u=0 MPa, e=1.44; ρ_d=1140 kg/m^3
Swelling $\Delta V/V$=43.4%
Swelling with water available at the outer radius confinement
Axial contact surfaces with friction ϕ=7°

Figures 7 and 8 show comparison between modelled and measured results.

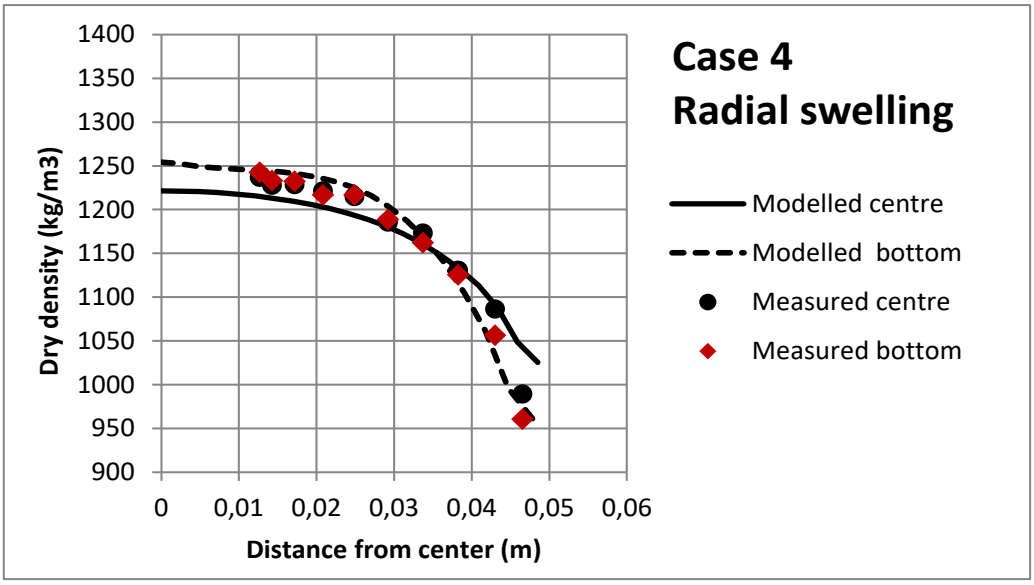

Figure 7: Modelled and measured dry density distribution.

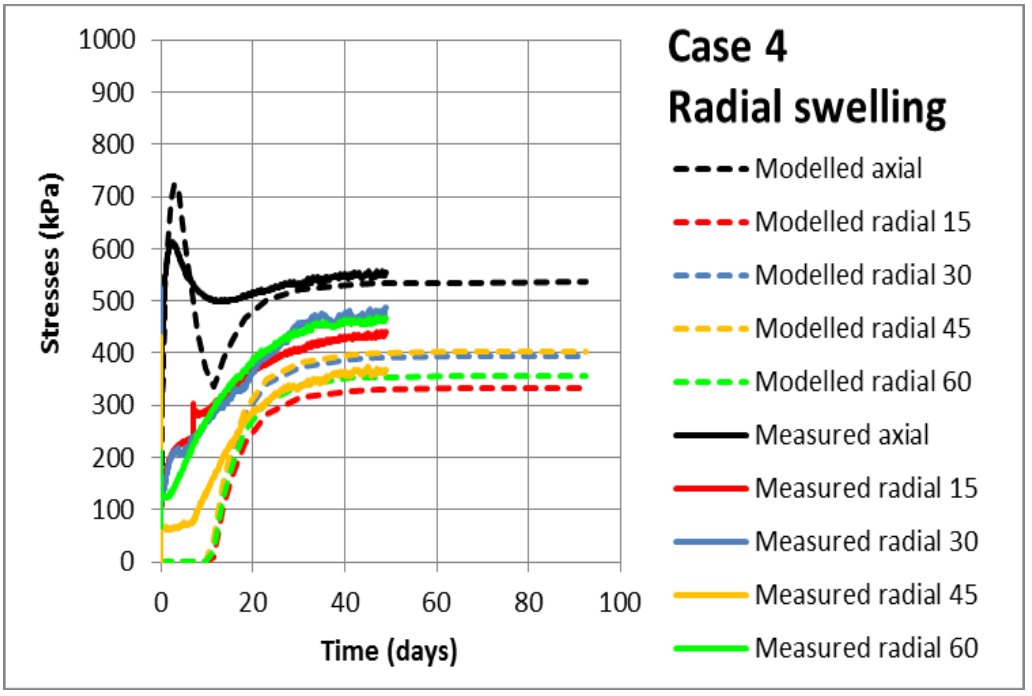

Figure 8: Modelled and measured evolution of stresses.

The comparison shows that although the calibration was done for the axial swelling test the agreement for the radial swelling is very good, even better than for the axial test. The measured dry density distribution is located between the two modelled parts. The influence of the boundaries (bottom and top lids) are also seen with a larger density drop in the bottom than in the middle, although the modelled results are more pronounced since the measurements include larger parts of the specimen.
The modelled and measured axial stress agrees very well although the peaks are smaller in the measurements. The same delay in modelled stress in the swelling direction as in test HRA1 is seen. The measured radial stresses are in average a little higher than the simulated.
In general, this simulation confirms the model.

3.4 Other fundamental swelling tests

Radial inwards swelling and isotropic swelling tests were also performed and modelled (Börgesson et al [2]). Both these models had problems and were not good due to numerical problems. At inwards swelling the central hole was not completely filled and at isotropic outwards swelling the density distribution was not well captured but isotropic swelling is not foreseen to take place.

4. Homogenisation in long tubes

4.1 Introduction

Tests of homogenisation in long tubes are ongoing with the purpose to investigate

- the ability of bentonite to homogenise in long tunnels or boreholes,
- the influence of friction between bentonite and different surface structures
- the long-term behaviour of large density differences

Ten tests with low density bentonite pellets in contact with high density compacted bentonite blocks installed in long steel tubes have started. In most tests, tubes with the diameter 26 mm and the length 250 mm were used. The tests are described and some results are reported by Dueck et al [7, 3, 1].

One of the tests (FLR5) has been terminated and sampled for determination of the density distribution two years after start. The other tests will be terminated after different times in order to see the influence of time on the homogenisation. The results from the terminated test and the results of measured evolution of swelling pressure in one of the tubes will be analysed in here. See also Dueck et al [3] and Börgesson et al [2].

The test set-up of FLR5 is shown in Figure 9. Half the tube is filled with highly compacted bentonite blocks with the diameter 25 mm and the other half with pellets. Swelling pressure is measured in four points, two in the pellet section and two in the high-density section, measuring axial and radial stress. Water is supplied through a filter at the top of the pellet section.

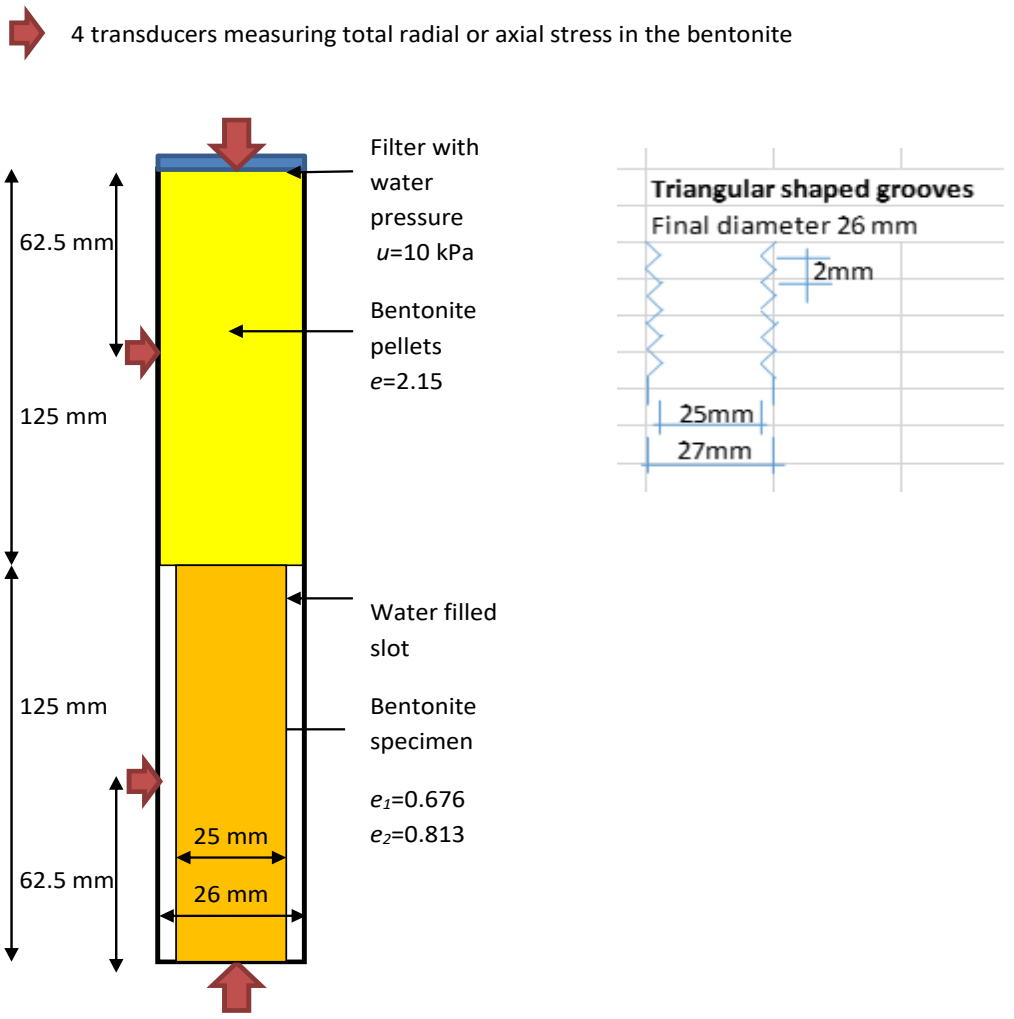

Figure 9: Geometry of the set-up and void ratios of the installed bentonite in test FLR5. e_1 is the void ratio of the blocks and e_2 is the final void ratio after radial swelling. The grooves in the inner surface of the tube is also illustrated.

The inner surface of the tube was grooved with 1 mm deep triangular groves yielding a diameter varying between 25 and 27 mm as shown in Figure 9. The average inner diameter of the tube is thus 26 mm.
The initial dry densities and corresponding void ratios are shown in Table 4. The swelling pressures are taken from Equation 2, derived by Börgesson et al [10] and has to be recalculated for high void ratios.

$$\sigma = \sigma_0 \cdot \left(\frac{e}{e_0}\right)^{\frac{1}{\beta}} \quad (2)$$

where
β=-0.19
e_0=1.1
σ_0=1000kPa
Equation 2 refers to non-saline water and MX-80 and is only valid for 0.5<e<1.5. The relation between void ratio and dry density is described by Equation 3.

$$\rho_d = \frac{\rho_s}{1+e} \tag{3}$$

where
ρ_d = dry density
e = void ratio
ρ_s = density of solids = 2780 kg/m^3

Table 4: Initial conditions for the bentonite in the tubes.

Section	Dry density [kg/m^3]	Void ratio	Swelling pressure kPa	Remarks
Pellet section	882	2.15	120[1)]	e>1.5
Pellet section[3)]	1 051[3)]	1.65	120[2)]	Recalculated
High density section	1 659	0.676	12 968[2)]	Installed
High density section	1 534	0.813	4 910[2)]	After radial swelling
1: Börgesson et al [10] 2: Equation 2 3: Apparent density to fit Equation 2				

Since the void ratio of the pellets is higher than 1.5 it had to be recalculated to fit Equations 2 in order to yield the initial expected swelling pressure 120 kPa. The test was analysed both analytically and numerically.

4.2 Analytical solution

The equilibrium state regarding the relation between swelling pressure and the friction between the bentonite and the walls in axial direction in a circular tube after completed swelling and compression can be derived and described according to Equations 4 and 5 (see e.g. Åkesson et al [8])

$$\sigma = \sigma_0 \cdot e^{\frac{-2z\tan\phi}{r}} \tag{4}$$

$$z = \frac{r}{2\tan\phi}\ln\frac{\sigma_0}{\sigma} \tag{5}$$

where

r = tube radius
z = axial distance from the bottom
σ_0 = swelling pressure at $z = 0$
σ = swelling pressure at z
ϕ = friction angle between the bentonite and the tube surface

The set-up is designed with the idea that the swelling of the high-density bentonite and the compression of the low-density bentonite will take place in the central parts of the tube and the difference in swelling pressure will be taken by the friction between the bentonite and the walls of the tube. The length of the tube is designed so that initial densities of the bentonite in the uppermost part of the pellet section and in the lowermost part of the high-density section shall remain intact and the density decrease will take place along the length L also called the transition zone, without affecting the end densities. Figure 10 illustrates the equilibrium state.

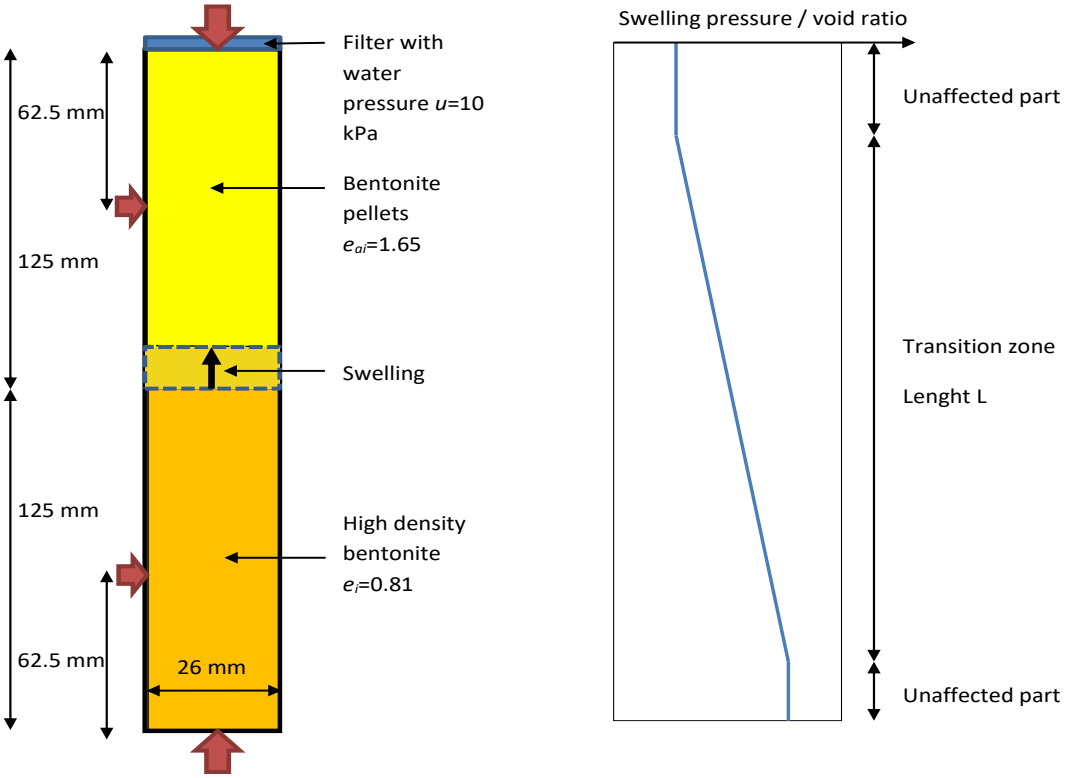

Figure 10: Illustration of the transition zone and the density and void ratio distribution after completed swelling.

In order to analyse the density distribution after equilibrium we need a relation between dry density and swelling pressure.

Combining Equations 2 and 3 yields the following initial swelling pressures for the high- and low-density sections by using the initial dry densities (as shown in Table 4):

- High density section (before radial swelling) σ=13.0 MPa
- High density section (after radial swelling) σ=4.9 MPa
- Pellet section (Börgesson et al [10]) $\sigma\approx$120 kPa

In order to be able to use Equations 2 and 4 for the pellet filling we must apply an apparent density and void ratio that yields the swelling pressure 120 kPa. Table 4 also shows those values.
The equilibrium in axial direction after swelling can be modelled according to Equations 2 to 5. Combining Equations 2 and 4 for the swelling pressure yields Equation 6.

$$\sigma_r \left(\frac{e}{e_r} \right)^{\frac{1}{\beta}} = \sigma_0 \cdot e^{-\frac{2z\tan\phi}{r}} \tag{6}$$

Applying Equation 3 for the relation between void ratio and dry density and
e_r=1.1 = reference void ratio
σ_r =1000 kPa = reference swelling pressure at e_r=1.1
yields Equation 7:

$$1000 \cdot \left| \frac{\left(\frac{\rho_s}{\rho_d} \right) - 1}{1.1} \right|^{\frac{1}{\beta}} = \sigma_0 \cdot e^{-\frac{2z\tan\phi}{r}} \tag{7}$$

$$\frac{\frac{\rho_s}{\rho_d} - 1}{1.1} = \left(\frac{\sigma_0}{1000} \cdot e^{-\frac{2z\tan\phi}{r}} \right)^{\beta} \tag{8}$$

$$\frac{\rho_s}{\rho_d} = 1.1 \cdot \left(\frac{\sigma_0}{1000} \right)^{\beta} \cdot e^{-\frac{2z\tan\phi}{r}\beta} + 1 \tag{9}$$

Applying β = -0.19, r = 0.013 m and ρ_s = 2.78 t/m^3 yields

$$\frac{2780}{\rho_d} = 1.1 \cdot \left(\frac{\sigma_0}{1000} \right)^{-0.19} \cdot e^{\frac{0.38 \cdot z \cdot \tan\phi}{0.013}} + 1 \tag{10}$$

$$\rho_d = \frac{2780}{1.1 \cdot \left(\frac{\sigma_0}{1000}\right)^{-0.19} \cdot e^{29.2 \cdot z \cdot \tan\phi} + 1} \tag{11}$$

Applying the initial swelling pressure at the high-density zone σ_0=4910 kPa yields the dry density distribution.

$$\rho_d = \frac{2780}{0.810 \cdot e^{29.2 \cdot z \cdot \tan\phi} + 1} \tag{12}$$

The length L of the transition zone can thus be derived by inserting the dry density of the pellet filling ρ_d=1051 kg/m^3.

$$0.810 \cdot e^{29.2 \cdot z \cdot \tan\phi} = \frac{2780}{\rho_d} - 1 \tag{13}$$

$$e^{29.2 \cdot z \cdot \tan\phi} = \left(\frac{2780}{1051} - 1\right) / 0.810 \tag{14}$$

$z=L=0.0243/\tan\phi$ (15)

Equation 12 thus yields the dry density distribution along the tube axis after force equilibrium and Equation 15 yields the length of the transition zone. Observe though that the dry density at void ratios higher than 1.5 (or dry densities lower than 1112 kg/m^3) are incorrect and must be adjusted.
The void ratio distribution can be calculated combining Equation 3 and Equation 12 yielding

$$e = 0.810 \cdot e^{29.2 \cdot z \cdot \tan\phi} \tag{16}$$

and the swelling pressure distribution can be calculated by inserting Equations 16 into Equation 17 (same as Equation 4).

$$\sigma = \sigma_r \left(\frac{e}{e_r}\right)^{\frac{1}{\beta}} \tag{17}$$

The influence of the friction angle on the length of the transition zone according to Equation 15 is shown in Figure 11. The dry density distribution, the void ratio distribution and the swelling pressure distribution as function of the distance from the intact high-density part (z) are shown for different friction angles in Figures 12, 13 and 14.

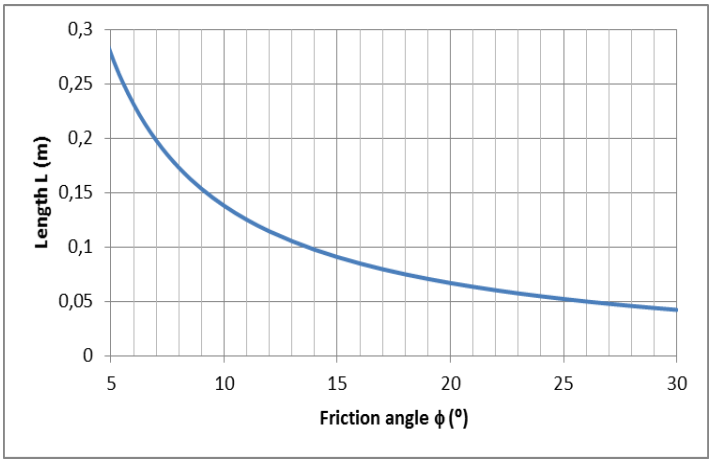

Figure 11: The length of the transition zone L as a function of the friction angle according to Equation 15.

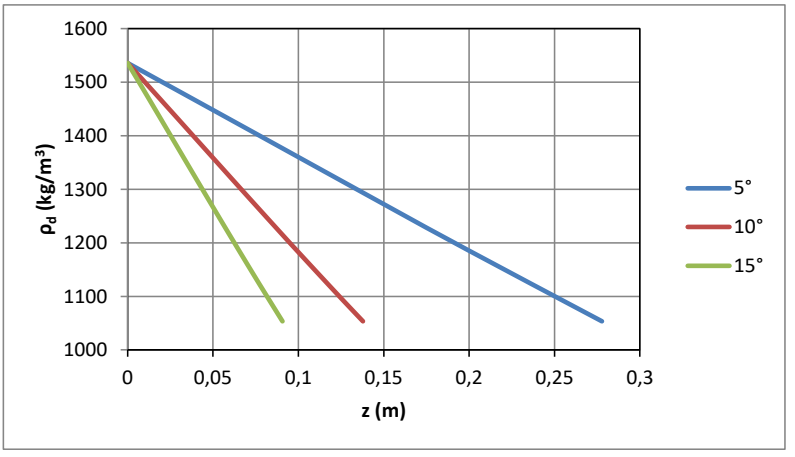

Figure 12: Dry density distribution of the transition zone at different friction angles according to Equation 12.

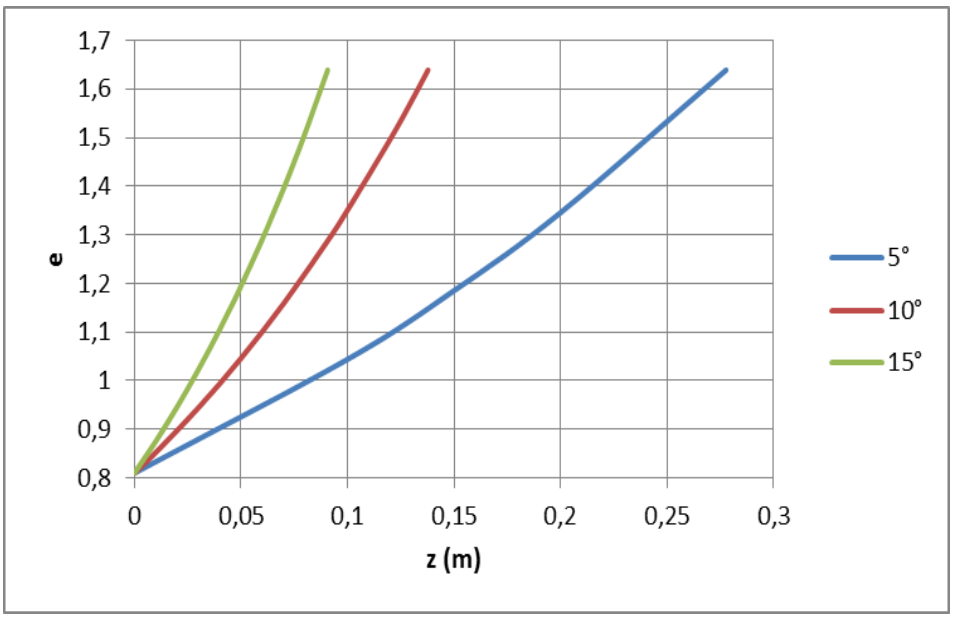

Figure 13: Void ratio distribution of the transition zone at different friction angles according to Equation 16.

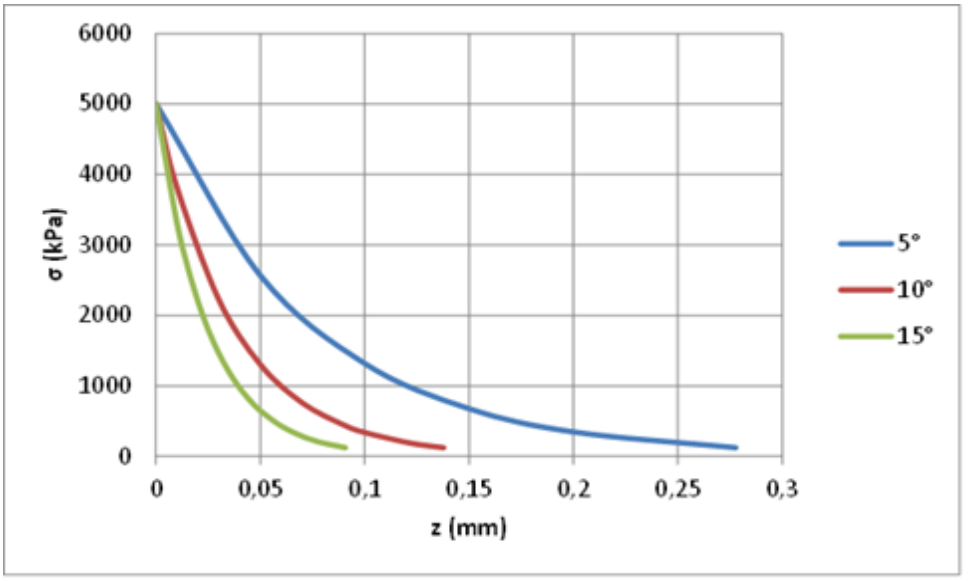

Figure 14: Swelling pressure distribution of the transition zone at different friction angles according to Equations 16 and 17.

The measured dry density distribution is shown in Figure 15.

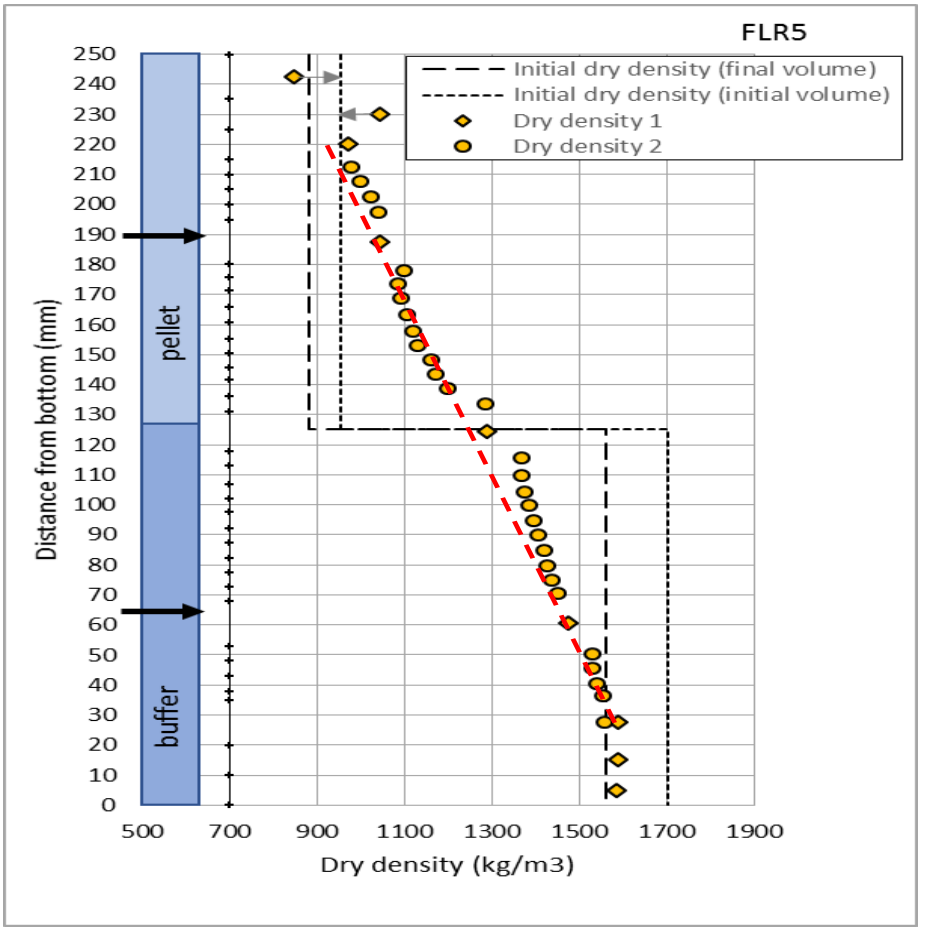

Figure 15:Measured dry density distribution of test FLR5. Dry density 1 is actual measured dry density. Dry density 2 is back-calculated dry density from the water ratio assuming 100 % degree of saturation.

Adapting a linear relation of the measured dry density distribution in Figure 15 yields the dashed line reaching between 27 mm and 220 mm (red hatched line) or a transition zone with the length 193 mm.

The swelling pressure was not measured in test FLR5. However, it was measured in test FLR2 (see Dueck et al [1]), which is identical to test FLR5. The swelling pressures at termination are compiled in Table 5.

Table 5: Swelling pressure from test FLR2 measured with a similar set-up as FLR5 at a time corresponding to the termination of test FLR5.

Type	Distance [mm]	Swelling pressure [kPa]	Direction
pellet	250	179	axial
pellet	187.5	247	radial
block	62.5	3381	radial
block	0	6231	axial

The test FLR5 was also modelled with Abaqus, see Dueck et al [3].

5. Discussion and conclusions

The average friction angle between the bentonite and the raw tube surface can be calculated from the measured length of the transition zone L=0.193 m according to Equation 15, which yields the average friction angle ϕ=7.2º.
However, the measured swelling pressure at the time for termination of FLR5 and the density measured deviate a little from the values used in the calculation.
The measured and modelled swelling pressures are compared in Table 6.

Table 6: Modelled swelling pressure and measured from test FLR2 with a similar set-up as FLR5 at a time corresponding to the termination of test FLR5.

Section	Distance [mm]	Direction	Measured ρ_d [kg/m^3]	Measured σ_a [kPa]	Modelled ρ_d [kg/m^3]	Modelled σ_a [kPa]
pellets	250	axial	950	179	1051	120
HCB	0	axial	1580	6231	1534	4910

Applying the measured swelling pressures and length of the transition zone into Equation 5 yields the average friction angle 6.8º, which is similar but slightly lower than derived from the first model.
The modelling and the comparison between modelling results and measured results from the long tube tests show that the understanding of the homogenisation processes is quite good. The rather simple analytical model of the tube with a swelling of the high-density zone and compression of the pellet zone that is counteracted by friction between the bentonite and the walls of the tube seems to be a very relevant way of predicting the final state of equilibrium and the distribution of bentonite density along the tube.
The results of the measurements and the calculations gave an average friction angle between the bentonite and the inner grooved surface of the steel tube of about ϕ=7º. Figure 16 shows the measured friction angle between MX-80 bentonite and different surfaces (Dueck et al [6]) as a function of the pressure.

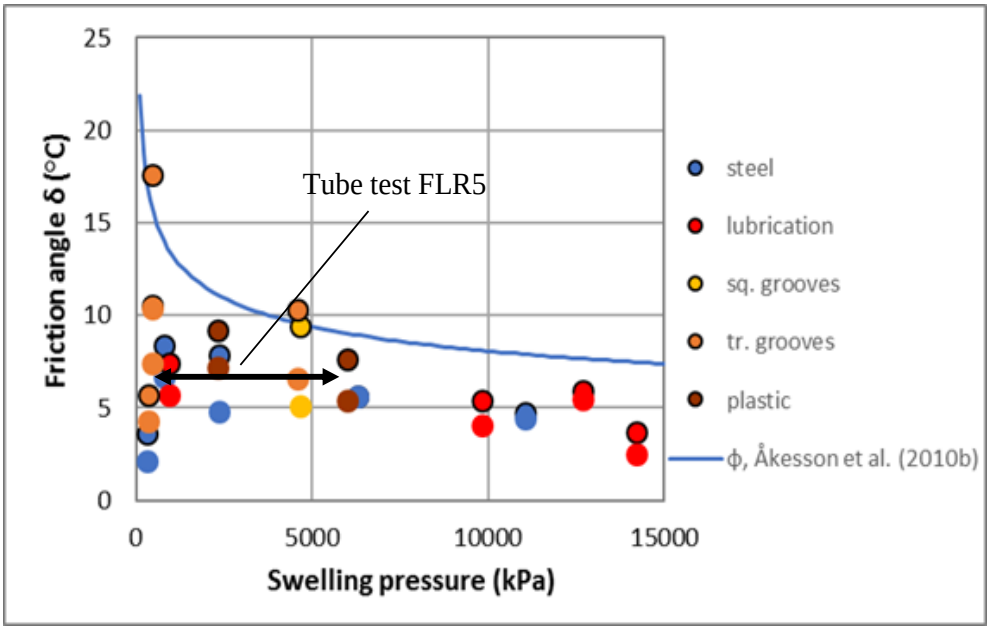

Figure 16: Measured friction angle between different bentonites and different surface structures. The different colors correspond to different surfaces. The marks with borders are peak values and the marks without border are residual values. The black line arrow marks evaluated friction angle and the swelling pressure distribution along the steel tube for test FLR5. The blue line is the measured inner friction angle of MX-80.

In Figure 16 the evaluated results of test FLR5 are included. The surface of the steel tube in that test corresponds to the tests with grooves marked with yellow and orange marks of the friction tests. It is obvious that the peak values (marks with borders) of those grooved surfaces correspond well to the internal friction angle of the bentonite materials, which is logical since there has to be a failure in the bentonite for start sliding. The residual values are close to half the peak values. The results of the test FLR5 agree rather well with the residual values. This is also logical since there has to be a sliding in order to start swelling and homogenisation.

One open question mark has been if the swelling is so slow that the peak strength of the bentonite is regained during the homogenisation. The results from test FLR5 clearly indicates that this is not the case. The conclusion is thus that the residual friction angles, corresponding to about half the internal friction angle in the bentonite, shall be used for homogenisation calculations even if a very raw surface is present.

6. Modelling of the Self-Healing Test SH1

6.1 Test setup

The Self-Healing test SH1 has been modelled as Subtask 2 of the homogenisation task of phase 2 of the TF EBS. The test and some results are described by Dueck et al [7, 1] and modelling of the test is described by Börgesson et al [2].

The test concerned swelling and self-healing of two cavities with the dimensions 35x50x70 mm cut in a bentonite block with the diameter 300 mm and the height 100 mm. The test layout is shown in Figure 17. The test included measurement of swelling pressure in 9 positions and suction in 2 positions. The test was terminated after equilibrium and vastly sampled after for 2 years and 8 months. The density and water ratio of the samples were determined.

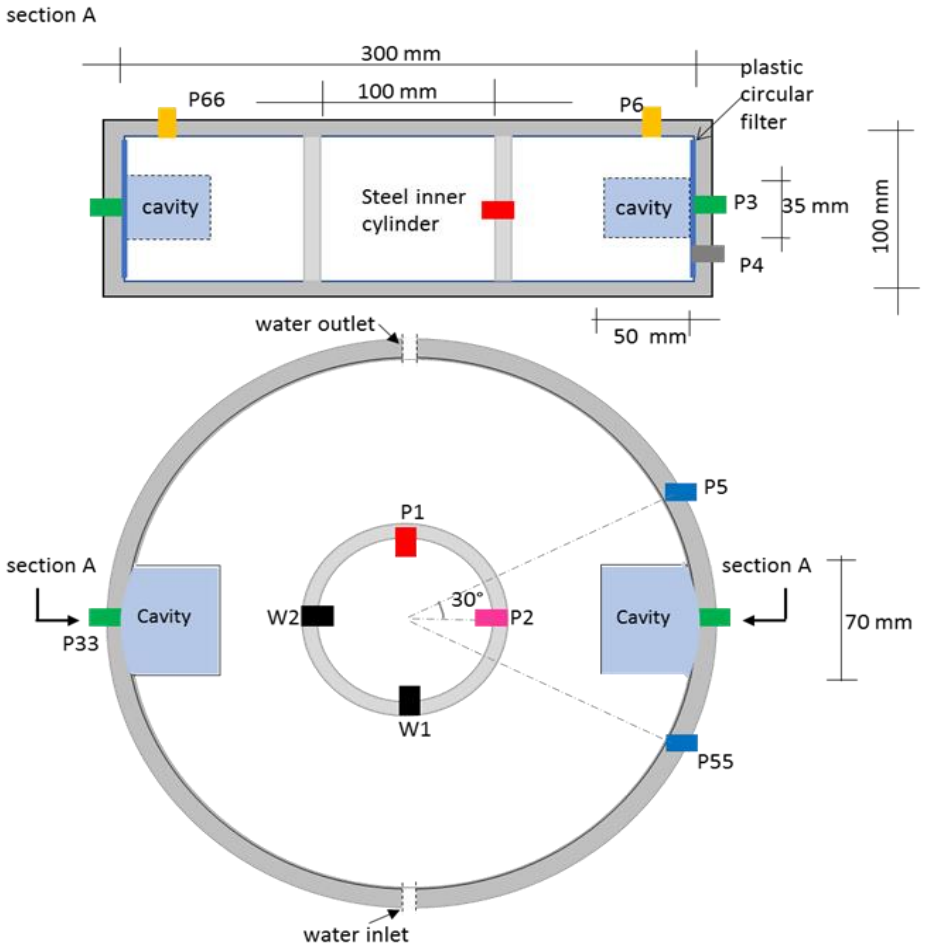

Figure 17: A sketch showing the layout of the test SH1 and the location of the transducers.

7. Calculations

A blind prediction was done and delivered before start of the test with the finite element code Abaqus. The new Claytech Plastic Cap material model that had been calibrated and verified in tests HRA1 and HR-Ro1 was used for the prediction. The test was also modelled using the Drucker-Prager plastic material model that had been used for SR-Site. The material models and the parameter values were shown earlier in this article. The steel cylinders and the end lids are modelled as linear elastic with standard values of steel properties.

The element mesh was simplified to cover only $1/8^{th}$ of the bentonite block by using symmetry planes. Figure 18 shows the block before installation in the steel confinement and the element mesh used in the FEM calculation.

The contact between the bentonite specimen and the surrounding steel tube and filter has been modelled with the friction angle ϕ_c=5º, which agrees well with the measurements shown in Figure 16 for the swelling pressure 5-10 MPa.

The bentonite is assumed to be completely water saturated from start but without swelling pressure against the walls. The swelling pressure is instead taken by a negative pore water pressure, which means that the total stress initially is zero.

e_0 = 0.70
p_0 = 10000 kPa
u_0 = -10000 kPa

The initial value of the water pressure -10000 kPa is ramped down to 0kPa in 10000 seconds in the nodes of the cylinder wall surface where water was supplied through the filter and in the surface nodes of the cavities (simulating water filled cavity). The calculation was run for 3.17 years (10^8 seconds). In order to improve the ability of the calculation to converge, a process that stabilizes the calculation by adding damping with counterforces was used.

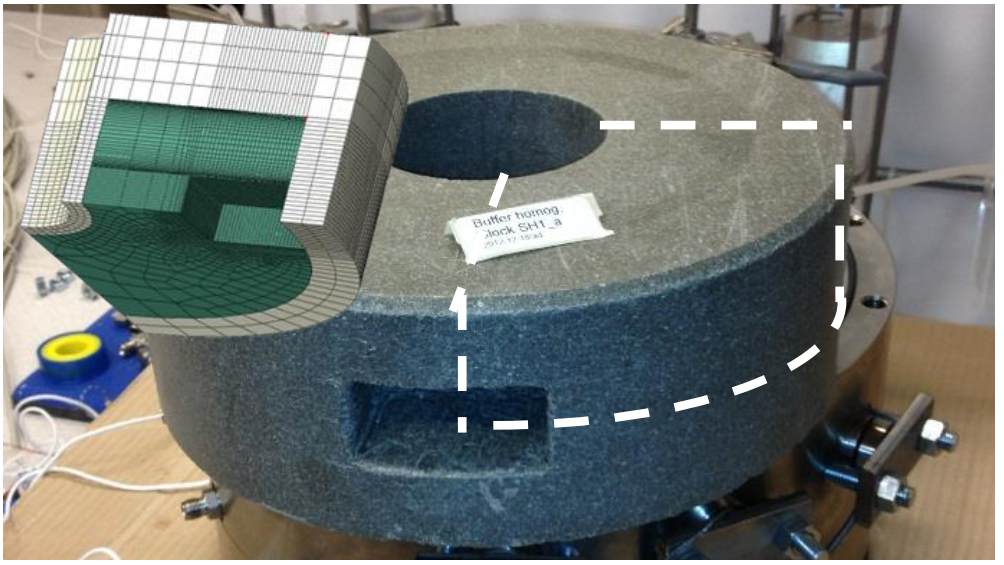

Figure 18: Illustration of how the 1/8th part of the bentonite block is used in the element mesh. The mesh is shown upper left. The green part of the mesh corresponds to the bentonite.

The SH1 test was started on December 18, 2012, in the afternoon by filling the filters and the cavities with water and applying a low water pressure (10kPa). The modelling that is described was done in November 2012, the figures plotted on December 12 and a PM describing the calculation was delivered before start of the test. So, it was a true blind prediction.

8. Results

8.1 Transducer measurements

Figure 19 shows the measured and modelled total stresses in the prediction. The comparison of the end values clearly shows that the modelled stress 2MPa in the center of the cavity (P3) is lower than the measured stress 3.3MPa. On the other hand, the stress at the inner steel cylinder P1 is overestimated by the modelling (9.7MPa) compared to the measured stress 6MPa. The modelled stress that agrees best with the measured is at the lid above the cavity (transducers P6 and P66) where the modelled stress is 4.0MPa and the measured stresses are 3.8MPa and 4.5MPa.

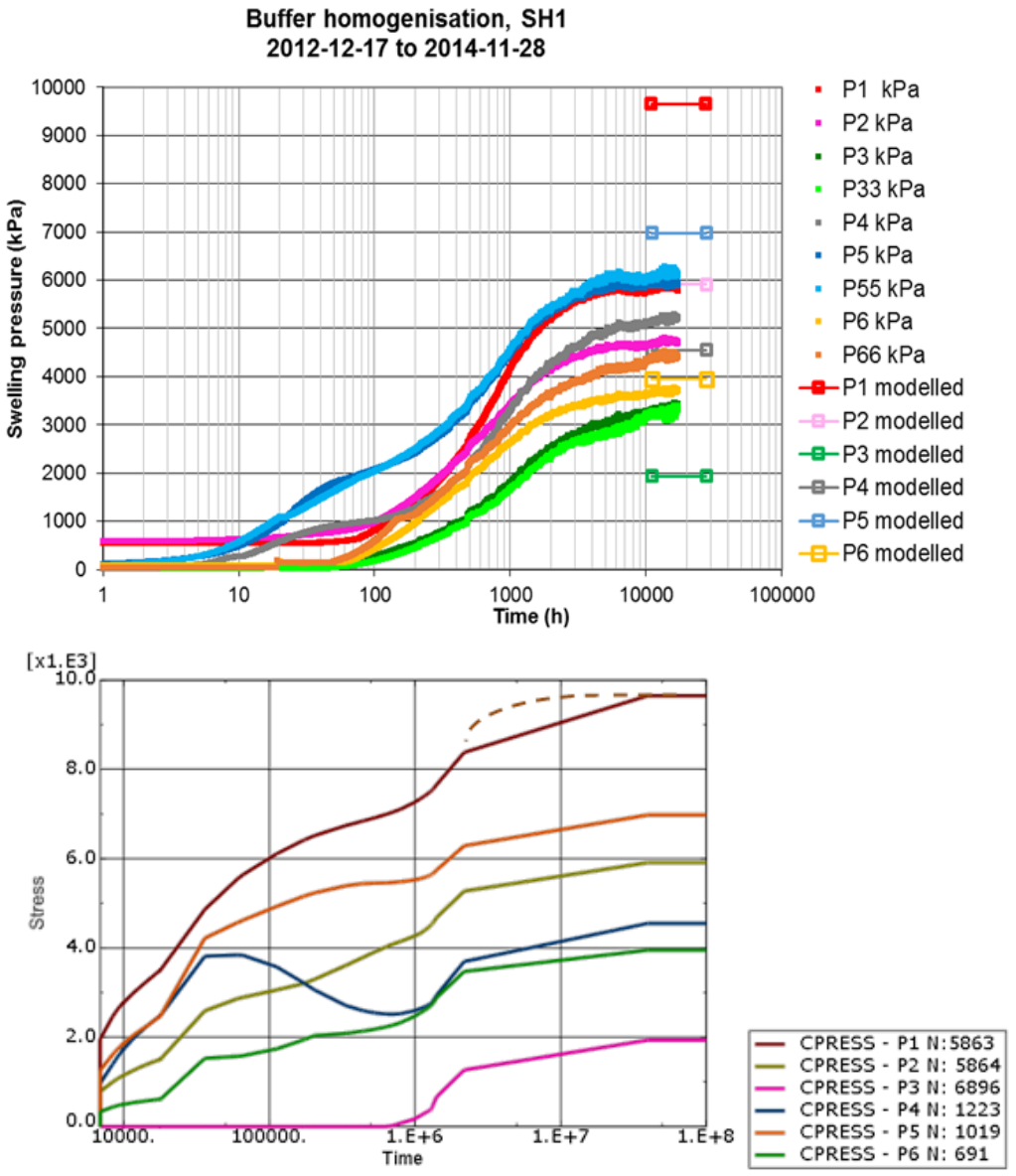

Figure 19: Measured and modelled stress evolution. The upper diagram shows the measured evolution and the final values of the modelled stresses. The lower diagram shows the modelled evolution (time in seconds and pressure in kPa). The time scale is the same in the two diagrams in the sense that 10^8 s corresponds to about 28 000 hours. See Figure 17 for the location of the transducers.

The measured time evolution seems to be slower than the modelled. Unfortunately, the modelling data is missing when the stresses reach their final values, but an estimate yields that the modelled homogenization goes 2-3 times faster than the measured. This is confirmed by the stress at P6 (which agreed well between measured and modelled final stress). The modelled stress at P6 is 3.5MPa after about 700 hours, while the measured stress 3.5MPa is reached after about 2000 hours.

The too fast modelled homogenization can partly be explained by the fact that the model assumes complete water saturation from start and no slots between the bentonite block and the boundaries. However, the actual bentonite block was only saturated to about 95% and the block did not completely fill up the space between the inner and outer cylinder. So, there was a need for extra water to be transported into the bentonite both for saturation and for swelling, which delays the time to equilibrium.

8.2 Density distribution

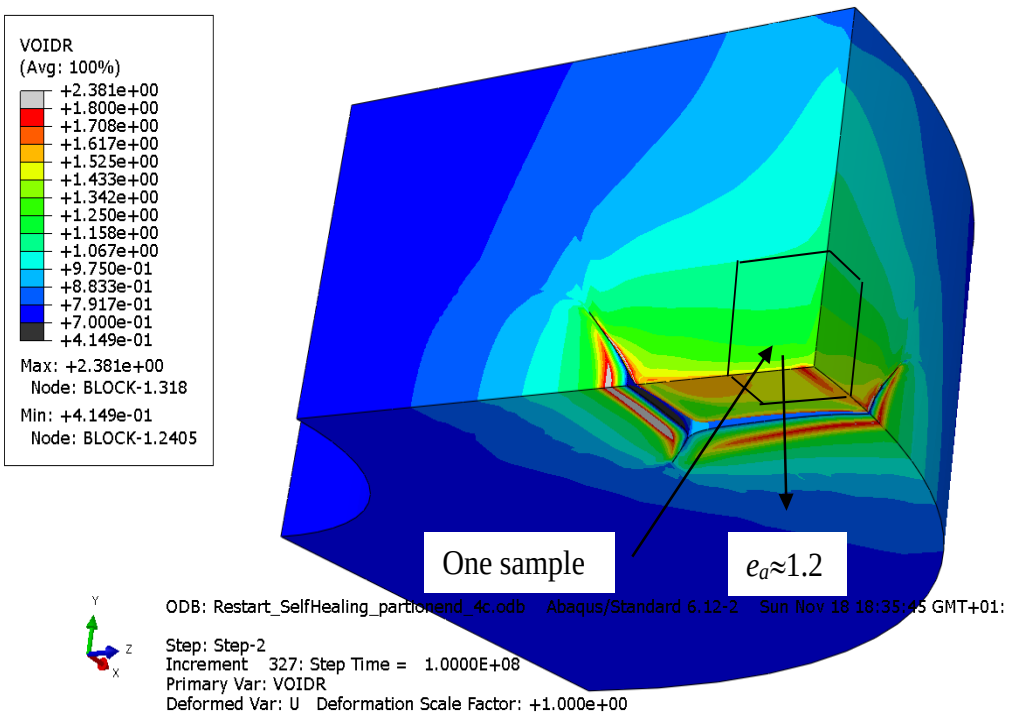

Figure 20. Modelling of the self-healing of the cavity. The picture shows the modelled void ratio distribution after completed homogenization. The size of one sample taken after the test is illustrated. The evaluated average void ratio of that part is e_a≈1.2.

The measured void ratio distribution in the central section is shown in Figure 21.

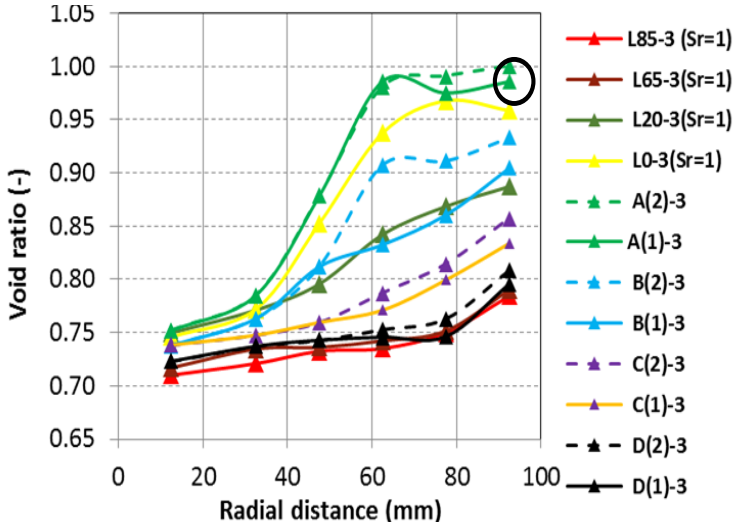

Figure 21: Measured void ratio distribution in the central section. The encircled value corresponds to the sample shown in Figure 20. For more information about the measured results see Dueck et al [1].

The extension of the sample shown in Figure 20 is so large that the modelled void ratio varies between about $1.8<e<1.0$. An evaluation of the average void ratio yields $e_a \approx 1.2$. This sample corresponds to the measured result encircled in Figure 21, which has $e=1.0$. The modelling thus overestimates the void ratio, which agrees with the modelled too low radial stress at corresponding location where the total stress was measured with transducers P3 and P33 (2.0MPa compared to the measured 3.3MPa).

9. Conclusion

A general conclusion is thus that the Claytech Plastic Cap model could model the homogenisation process but underestimated the self-healing ability of the bentonite in the test by yielding too high void ratio and too low stresses in the former cavity.

9.1 Analyses and conclusions

Four different types of homogenisation tests have been modelled. Three of them have been modelled with the FEM program Abaqus and one has been modelled with an analytical model.

The HR (high resolution) tests have been modelled with two different mechanical material models. The models have the same porous elastic model for simulating the non-linear isotropic swelling and compression of bentonite, but they have different plastic models for simulating the effect of deviatoric stresses. The Drucker-Prager model is a classic material model included in the model library of Abaqus. The other

model (Claytech Plastic Cap model) has been implemented in Abaqus.
The HR-test with only axial swelling was used to check and calibrate the parameters of the models. Then the HR-test with only radial swelling was modelled with the calibrated parameters. Both tests were very well modelled with the Claytech Plastic Cap model but less good with the Drucker-Prager model.
The conclusion of these exercises and additional tests that were modelled, was that the Claytech Plastic Cap model simulates bentonite swelling well within a limited density interval but also that the model probably does not work well for the unlikely case of completely isotropic swelling. In addition, closing of cylindrical and spherical holes are not well modelled due to numerical problems with strongly deformed elements.
The Claytech Plastic Cap model was then used to model the Self-Healing test SH1 with a true prediction. SH1 included swelling and homogenisation of a large bentonite block with two cavities. The modelling worked well but the Claytech Plastic Cap model underestimated the self-healing ability (or the homogenisation) of the bentonite in the test by yielding too high void ratio (20%) and too low stresses (40%) in the former cavity.
Ten almost identical tests of the homogenisation of two bentonites with large density differences placed in long tubes with raw surfaces have been running for 4-5 years with the purpose to study the long-term homogenisation process.
The test was modelled with a simplified analytical model that studies the equilibrium after completed homogenisation. Back-calculating the friction angle from this model yielded the value ϕ=7º, which gave very good agreement between modelled and measured density distribution. This value also agrees with the average residual friction angle received from friction tests that measure the shear resistance between bentonite and the same type of raw surface. An important conclusion from these tests is thus that it is the residual friction angle and not the peak value that is valid between a bentonite and a surface even when the surface is so raw that the slip takes place in the bentonite itself.

ACKNOWLEDGEMENTS.
The study is funded by the Swedish Nuclear Fuel and Waste Management Company (SKB).

References

[1] Dueck, A., Börgesson, L. and Goudarzi, R. (2019). Bentonite homogenisation – laboratory study of homogenisation processes in buffer and backfill materials in repositories. Journal of Earth Sciences and Geotechnical Engineering, London. Special Issue on Disposal of Radioactive Waste Using Clay Barriers. 2019.

[2] Börgesson, L., Hernelind, J. and Åkesson, M. (2018). EBS TF - THM modelling. Homogenisation task. SKB P-18-05. Svensk Kärnbränslehantering AB.
[3] Dueck, A., Börgesson, L., Hernelind, J., Kristensson, O., Malmberg, D. and Åkesson, M. (2018). Bentonite homogenisation. Laboratory study, model development and modelling of homogenisation processes. SKB TR-19-11. Svensk Kärnbränslehantering AB.
[4] Dueck, A., Goudarzi, R. and Börgesson, L. (2011). Buffer homogenisation, status report. SKB TR-12-02. Svensk Kärnbränslehantering AB.
[5] Dueck, A., Goudarzi, R. and Börgesson, L. (2014). Buffer homogenisation, status report 2. SKB TR-14-25. Svensk Kärnbränslehantering AB.
[6] Dueck, A., Goudarzi, R. and Börgesson, L. (2016). Buffer homogenisation, status report 3. SKB TR-16-04. Svensk Kärnbränslehantering AB.
[7] Dueck, A., Goudarzi, R. and Börgesson, L. (2017). Buffer homogenisation, status report 4. SKB TR-17-04. Svensk Kärnbränslehantering AB.
[8] Åkesson, M., Kristensson, O., Börgesson, L., Dueck, A. and Hernelind, J. (2010).THM modelling of buffer, backfill and other system components. Critical processes and scenarios. SKB TR-10-11. Svensk Kärnbränslehantering AB.
[9] Åkesson, M., Börgesson, L. and Kristensson, O. (2010). SR-site Data report, THM modelling of buffer, backfill and other system components. SKB TR-10-44. Svensk Kärnbränslehantering AB.
[10] Börgesson, L., Johannesson, L.E., Sandén, T. and Hernelind, J. (1995). Modelling of the physical behaviour of water saturated clay barriers. Laboratory tests, material models and finite element application. SKB TR-95-20. Svensk Kärnbränslehantering AB.
[11] Börgesson, L., Åkesson, M., Birgersso,n M., Hökmark, H. and Hernelind, J. (2013a). EBS TF - THM modelling. BM 1: small scale laboratory tests. SKB TR-13-6. Svensk Kärnbränslehantering AB.
[12] Börgesson, L., Åkesson, M., Kristensson, O., Malmberg, D., Dueck, A. and Hernelind, J. (2013b). EBS TF – THM modelling of BM 2: Large scale field tests. SKB TR-13-7. Svensk Kärnbränslehantering AB.